Insights into the possible existence of a soft dipole mode in ^{8}He

J. Piekarewicz*
Department of Physics, Florida State University, Tallahassee, Florida 32306, USA

(Received 9 February 2022; accepted 23 March 2022; published 12 April 2022)

With an extreme neutron-to-proton ratio of $N/Z = 3$, ^{8}He provides an ideal laboratory for the study of a variety of exotic phenomena, such as the emergence of a soft dipole mode that is dominated by transitions into the continuum. In this contribution, a covariant density-functional theory (DFT) framework is used to compute ground-state properties and the dipole response of ^{8}He. Although ^{8}He is admittedly too light for DFT to be applicable, the great merit of the approach is that the spurious contamination associated with the center-of-mass motion is guaranteed to decouple from the physical response. Given that a strong mixing between the isoscalar and isovector dipole modes is expected for a system with such a large neutron-proton asymmetry as ^{8}He, the narrow structures that emerged at low energies in the isovector dipole response are attributed to the shift of the spurious strength to zero (or near zero) excitation energy. Thus, the theoretical framework implemented here disfavors the emergence of a soft dipole mode in ^{8}He.

DOI: 10.1103/PhysRevC.105.044310

I. INTRODUCTION

Which combinations of neutrons and protons can form a bound atomic nucleus is one of the overarching questions animating nuclear science today [1]. A core mission of nuclear science is to map the neutron drip line, which requires the identification of the most neutron-rich element in an isotopic chain that remains stable against particle decay. So far, the neutron drip line has been mapped up to an including fluorine and neon [2]—a challenging experimental task that took almost two decades since the confirmation of ^{24}O as the $Z = 8$ dripline nucleus [3,4]. In the case of helium, the last stable isotope is ^{8}He—an exotic nucleus with an extreme neutron-to-proton ratio of $N/Z = 3$; see Ref. [5] and references therein. Among the novel behavior that emerges at the limits of stability is the development of neutron halos and neutron skins, due to either a low neutron separation energy or a large neutron-proton asymmetry. Besides the development of extended spatial distributions, weakly bound nuclei often give rise to soft modes of excitation that involve transitions into the continuum.

An early experiment using the Coulomb excitation of ^{8}He identified a soft dipole resonance at an excitation energy of about 4 MeV [6,7]. Later on, Golovkov, Grigorenko, and collaborators populated the low-lying spectrum of ^{8}He via a transfer reaction and confirmed the existence of a soft dipole mode, albeit at a slightly lower energy of about 3 MeV [8,9]. In contrast, one of the main findings of the dissociation experiment on ^{8}He performed at Michigan State University concluded that an insignificant fraction of no more than 3% of the energy-weighted sum rule is exhausted by the low-energy mode [10]. This result has been validated by the recent inelastic proton-scattering experiment that concluded that the measured angular distribution is not consistent with a dipole excitation [11]. It is anticipated that the high statistics experiment already finalized at the RIKEN facility in Japan will settle the issue [12].

From the theoretical perspective, ground-state properties of ^{8}He have been computed using a variety of state-of-the-art *ab initio* methods [11,13–15]. However, to our knowledge, it is only the very recent *ab initio* work by Bonaiti, Bacca, and Hagen [15] that addresses the possible existence of a soft dipole mode in ^{8}He. The authors have merged the coupled-cluster framework to the Lorentz-integral-transform approach [16] to report on the emergence of low-energy dipole strength around 5 MeV, in agreement with Refs. [6–9], but in disagreement with Refs. [10,11].

In this paper I offer an alternative theoretical perspective based on density-functional theory. Density-functional theory (DFT) is a powerful technique developed by Kohn and collaborators [17,18], whose great merit is that the exact ground-state energy and one-body density of a complicated many-body system is obtained by minimizing a suitable energy density functional (EDF). To make the problem tractable, Kohn and Sham demonstrated how the complex interacting many-body system can be made equivalent to a system of noninteracting electrons moving in an external—mean-field-like—potential [18]. Among the advantages of the Kohn-Sham formulation is that self-consistent problems of this kind are routinely solved in many fields, including nuclear physics. Indeed, nuclear EDFs, although not always known as such, have a long and successful history in nuclear physics; see Ref. [19] and references therein. The widely used density-dependent Skyrme forces were developed almost a decade before the inception of density-functional theory [20,21]. In this paper a covariant formulation of DFT is implemented that is based on an extension of the work by Walecka, Serot, and many others [22]. For details of the particular implementation used in this work, see the recent review published in Ref. [23].

*jpiekarewicz@fsu.edu

Advocating in favor of mean-field-like approaches for light systems such as ^{8}He may come as a surprise. Although not a problem in the case of electrons bound to a heavy nucleus, the main problem with self-bound systems such as atomic nuclei is the absence of a natural external potential and a proper treatment of the center of mass (COM). Indeed, as pointed out by Engel [24], without a proper decoupling of the COM, the ground state of a self-bound system has a—manifestly incorrect—density that is uniformly distributed over space [19,24]. Among the treatments dealing with the removal of the COM contribution to the energy is an approach based on a harmonic-oscillator approximation. This prescription, which falls down slowly with mass number [25], makes a significant contribution to the energy of light nuclei—especially for those at the drip line. As such, large COM corrections to the energy hinder any meaningful prediction of the ground-state energy of light systems. However, the situation improves considerably when dealing with the linear response of the system. More than six decades ago in a seminal paper, Thouless showed how, in a self-consistent formulation, the spurious state associated with a uniform translation of the center of mass separates out cleanly from the physical modes by having its strength shifted to zero excitation energy [26]. This result is particular relevant for isoscalar dipole excitations that share the same quantum numbers as the center of mass. However, for neutron-rich nuclei such as ^{8}He, one expects a strong mixing between isoscalar and isovector dipole modes. It is the main goal of the present contribution to examine the impact of such a mixing on the emergence—or lack thereof—of a soft dipole mode in ^{8}He.

The paper has been organized as follows: In Sec. II a brief description of the covariant random-phase approximation (RPA) formalism used in this work is presented, paying special attention to the treatment of the continuum and the mixing between isoscalar and isovector modes. Self-consistent results are then presented in Sec. III for the ground-state properties and distribution of isovector dipole strength of ^{8}He. Finally, Sec. IV contains a summary of the main results.

II. FORMALISM

The energy density functional used in this work is based on the nonlinear model introduced in Ref. [27], supplemented by an isoscalar-isovector term that influences the dynamics of neutron-rich matter [28]. Although previously discussed in great detail elsewhere, see, for example, Ref. [29] and references therein, the interacting Lagrangian density is displayed for completeness:

$$\begin{aligned}\mathscr{L}_{\rm int} = \bar{\psi}\Big[g_{\rm s}\phi - \Big(g_{\rm v}V_\mu + \frac{g_\rho}{2}\boldsymbol{\tau}\cdot\mathbf{b}_\mu + \frac{e}{2}(1+\tau_3)A_\mu\Big)\gamma^\mu\Big]\psi \\ - \frac{\kappa}{3!}(g_{\rm s}\phi)^3 - \frac{\lambda}{4!}(g_{\rm s}\phi)^4 + \frac{\zeta}{4!}g_{\rm v}^4(V_\mu V^\mu)^2 \\ + \Lambda_{\rm v}\big(g_\rho^2\,\mathbf{b}_\mu\cdot\mathbf{b}^\mu\big)\big(g_{\rm v}^2 V_\nu V^\nu\big),\end{aligned} \tag{1}$$

where the isodoublet nucleon field ψ interacts through the exchange of photons (A_μ) and three "mesons" of diverse spin-isospin character: a scalar-isoscalar (ϕ) a vector-isoscalar (V^μ), and a vector-isovector ($\mathbf{b}_\mu$) [27]. Furthermore, to improve the predictive power of the model, various self-interacting meson terms have been added. Ground-state properties of the system—namely, single-particle energies and Dirac orbitals, one-body densities, and mean-field-like potentials—are obtained from a self-consistent solution of the Kohn-Sham equations [23].

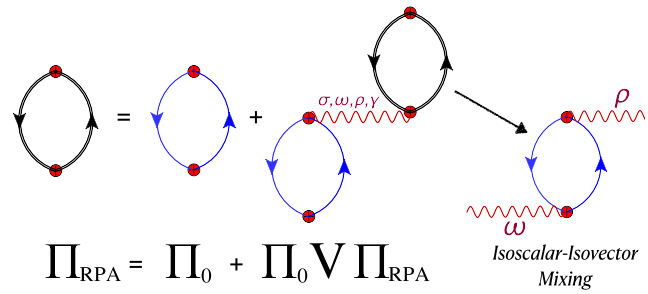

FIG. 1. Diagrammatic representation of the RPA equations. The bubble with the thick lines represents the fully correlated polarization tensor, while the one depicted with the thin lines is the uncorrelated polarization. The residual interaction denoted with the wavy line must be identical to the one used to generate the ground-state. The arrow in the figure indicates that the RPA bubble contains mixed contribution of various isospin and Lorentz structures.

Given that the Kohn-Sham equations may be derived from a variational approach, one can examine the small oscillations around the ground state. The consistent linear response of the ground state to an external perturbation is encapsulated in the RPA formalism that ensures that important symmetries are preserved [30,31]. Particularly critical to this work is the decoupling of the spurious state associated with a uniform translation of the center of mass [26].

The first step in generating the RPA response is the calculation of the uncorrelated polarization tensor, depicted by the thin (blue) bubble in Fig. 1. The spectral content of the uncorrelated polarization is both simple and illuminating: it contains simple poles at the single-particle excitations of the system with the associated transition densities obtained from the residues at the pole [30]. One obtains the RPA polarization tensor, depicted by the thick (black) bubble in Fig. 1, by iterating the uncorrelated polarization to all orders. If many particle-hole pairs with the same quantum numbers are involved, then the RPA response is strongly collective and one "giant resonance" tends to dominate, namely, the resonance exhausts most of the classical sum rule [32].

The diagrammatic structure of the RPA equations is depicted in Fig. 1. Two aspects of the RPA equations are particularly important. First, the wavy lines in the figure denote the residual particle-hole interaction. It is only by using a residual particle-hole interaction consistent with the interaction used to generate the mean-field ground state that the spurious strength associated with a uniform translation of the center of mass is decoupled from the physical response. Second, the variety of isospin and Lorentz structures of the residual interaction leads to a highly complex set of RPA equations. In particular, for nuclei with large neutron excess, the mixing of isoscalar and isovector modes is strong [31]. This is illustrated by the arrow in the figure that indicates that

the RPA bubble contains mixed isoscalar-isovector contributions. It is precisely such strong isoscalar-isovector mixing that will become critical in our interpretation of the emergence, or lack-thereof, of a soft dipole mode in ^{8}He.

I conclude this section by relating the distribution of isovector dipole strength $R(\omega)$ to the photoabsorption cross section and by defining various moments of the distribution. As shown in Ref. [33], $R(\omega)$ may be obtained from the dynamic longitudinal response, which is a function of both the excitation energy ω and the momentum transfer. In turn, the product $\omega R(\omega)$ is directly proportional to the photoabsorption cross section, namely,

$$\sigma_{\rm abs}(\omega) = \frac{16\pi^3}{9}\frac{e^2}{\hbar c}\omega R(\omega). \tag{2}$$

Often used in the literature are moments of the distribution of strength which are defined as follows:

$$m_n = \int_0^\infty \omega^n R(\omega) d\omega. \tag{3}$$

In particular, the energy-weighted sum m_1 satisfies a classical sum rule [32], whereas the inverse energy-weighted sum m_{-1} is proportional to the electric-dipole polarizability $\alpha_{\rm D}$[34]—a physical observables that has been shown to be a good isovector indicator [35,36]. That is,

$$m_1 = \frac{9\hbar^2}{8\pi M}\left(\frac{NZ}{A}\right) \approx 14.8\left(\frac{NZ}{A}\right){\rm fm}^2\,{\rm MeV}, \tag{4a}$$

$$\alpha_{\rm D} = \frac{\hbar c}{2\pi^2}\int_0^\infty \frac{\sigma_{\rm abs}(\omega)}{\omega^2}\,d\omega = \frac{8\pi e^2}{9}m_{-1}. \tag{4b}$$

III. RESULTS

Following the organizational scheme of Ref. [15], one starts this section by presenting results for the ground-state properties of ^{8}He followed by a discussion on the distribution of dipole strength. Predictions are made using three covariant energy density functionals: RMF016 (also known as "FSUGarnet"), RMF022, and RMF028 (or "FSUGold2") [37]. All three EDFs are identical in the isoscalar sector but differ in their isovector properties. Specifically, the EDFs were calibrated assuming different values for the (at the time) unknown value of the neutron skin thickness of ^{208}Pb. In particular, RMF016 was calibrated assuming a neutron skin thickness of 0.16 fm, RMF022 of 0.22 fm, and RMF028 of 0.28 fm. Based on the result published by the PREX Collaboration [38], namely, $R_{\rm skin}^{208} = 0.283 \pm 0.071$ fm, the RMF016 prediction falls within the two-sigma interval.

One should note that within the context of covariant DFT, all three accurately calibrated EDFs have been successful in describing a host of physical observables, such as ground-state properties of medium- to heavy-mass nuclei, their linear response, and the structure of neutron stars. Moreover, such EDFs have also been used to explore the evolution of the ground-state energy of the oxygen isotopes [37]. Whereas no lighter system than oxygen has been studied with this set of EDFs, it is interesting to explore their predictions for the isovector dipole response of ^{8}He, primarily due to the critical role that self-consistency plays in eliminating any spurious contamination.

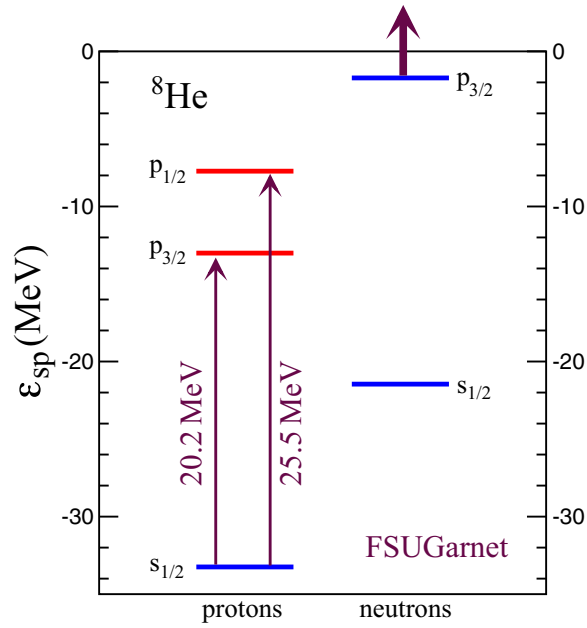

FIG. 2. Single-particle spectrum for ^{8}He as predicted by the covariant energy density functional FSUGarnet = RMF016. The blue (red) lines denote occupied (empty) orbitals and the thin arrows indicate discrete excitations into bound states. In turn, the thick arrow indicates that low-energy strength is expected to emerge from the excitation of the weakly bound neutron $p_{3/2}$ orbital into the continuum.

A. Ground-state properties

Self-consistent predictions for the bound single-particle spectrum of ^{8}He are displayed in Fig. 2, with the blue (red) lines indicating the occupied (vacant) single-particle orbitals. The two thin arrows indicate the two lowest "sharp" dipole transitions on the proton side. In contrast, all dipole excitations on the neutron side involve transitions into the continuum. Within the DFT framework employed here, the soft-dipole excitations indicated by the thick arrow involve the transition of the weakly bound $p_{3/2}$ orbital into the *sd* shell, which lies entirely in the continuum. These low-energy excitations will be discussed in greater detail in Sec. III B.

Listed in Table I are energies and root-mean-square radii (rms) for ^{8}He as predicted by the three models introduced earlier. The second column lists the single-particle energy of the $p_{3/2}$ neutron orbital, which displays a significant model dependence that is attributed to the difference in the isovector properties of the models. As shown in Fig. 3, the model with the stiffest symmetry energy (RMF028) generates the most attractive neutron potential at the large distances of relevance to the weakly bound $p_{3/2}$ orbital. Indeed, as indicated in the inset to Fig. 3, the $p_{3/2}$ orbital peaks at a distance of about 3.7 fm where the neutron potential generated by the RMF028 model is about 2 MeV deeper than the one generated by the model with the softest symmetry energy (RMF016). Note that the neutron potential is an effective Schrödinger-like potential

TABLE I. Predictions of a few ground-state properties of ^{8}He for the three models used in this work. The binding energy of the neutron $p_{3/2}$ orbital is compared against the experimental one-neutron separation energy listed in the National Nuclear Data Center database. The quoted experimental energy per nucleon was obtained from Refs. [39–41], the experimental charge radius from Ref. [42], while the derived quantities for R_p and R_n were extracted from Ref. [43].

Model	$\varepsilon(p_{3/2})$ (MeV)	E/A (MeV)	R_p (fm)	R_n (fm)	$R_n - R_p$ (fm)	$R_{\rm ch}$ (fm)	$R_{\rm wk}$ (fm)
RMF016	1.714	2.241–3.764	1.897	3.206	1.309	1.998	3.354
RMF022	2.740	2.521–4.044	1.883	3.023	1.140	1.981	3.175
RMF028	3.784	2.785–4.308	1.876	2.904	1.028	1.970	3.060
Experiment	2.535(8)	3.925	1.807(28)	2.73(9)	0.92(10)	1.929(26)	

obtained from a linear combination of the relativistic scalar and vector potentials [22].

The third column in Table I displays the binding energy per nucleon and makes abundantly clear one of the problems of using DFT for a light, self-bound system such as ^{8}He. The lower value listed on the table does not include any center-of-mass correction, while the higher value includes a significant COM correction of 1.52 MeV, obtained by assuming a harmonic-oscillator approximation [25]. Note that the lightest nucleus that was used in the calibration of the three covariant EDFs was ^{16}O [29,37], twice as heavy as ^{8}He.

The rest of the columns in Table I are predictions for rms radii. Based on the statistical analysis carried out in Ref. [29], an error of at least 0.03 fm should be attached to all theoretical predictions. Although several "experimental" values are listed in the table, only the charge radius of ^{8}He can be regarded as a model-independent determination [39,42,44]. Instead, the proton radius R_p quoted in Table I requires the unfolding of the finite proton size [43]. However, as indicated in Eq. (19) of Ref. [45], the charge radius includes spin-orbit contributions that go above and beyond the finite size of the proton. In the case of the experimental neutron radius quoted in Table I, it was obtained from both R_p and a determination of the matter radius from an elastic proton-scattering experiment [43]. However, besides the inherent uncertainties involved in the determination of nuclear radii using hadronic probes [46], the determination of R_n is also hindered by the uncertainties in the extraction of R_p mentioned above.

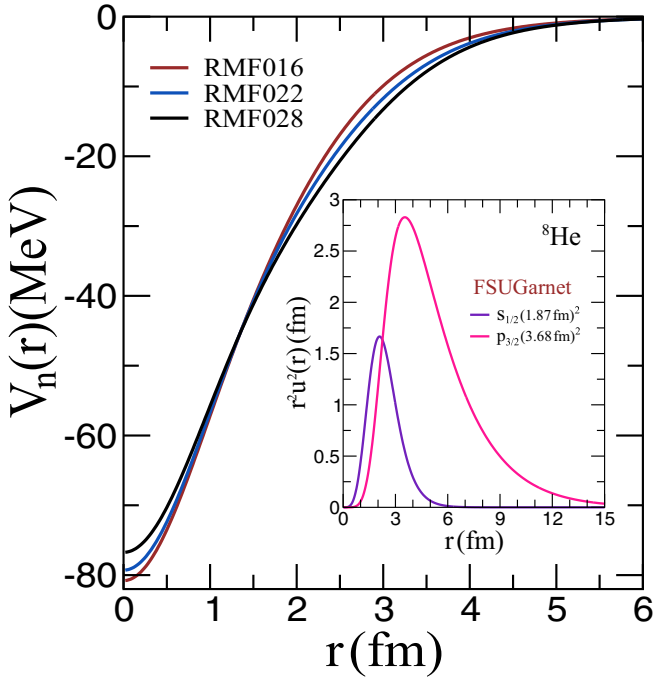

FIG. 3. Effective "Schrödinger-like" neutron potential for the three models considered in this work. The inset shows the two bound neutron orbitals in ^{8}He supported by the RMF016 = FSUGarnet potential and illustrates the large spatial extent of the $p_{3/2}$ orbital.

Within the context of density-functional theory and the Kohn-Sham equations, one has access to the entire spatial distributions, from which radii—as well as any other moment of the distribution—may be computed. Proton, neutron, charge, and weak-charge densities are displayed in Fig. 4(a) as predicted by FSUGarnet = RMF016. Note that both the charge and weak-charge densities incorporate spin-orbit corrections as outlined in Ref. [45]. In all four cases the spatial distribution can be accurately fit by a one-parameter Gaussian form. For example, in the case of the charge density and its associated form factor one obtains

$$\rho_{\rm ch}(r) = \left(\frac{3Z}{2\pi R_{\rm ch}^2}\right)^{3/2} e^{-3r^2/2R_{\rm ch}^2}, \tag{5a}$$

$$F_{\rm ch}(q) = e^{-q^2R_{\rm ch}^2/6}, \tag{5b}$$

where Z is the nuclear charge, $R_{\rm ch}$ is the charge radius of the distribution, and the form factor has been normalized to

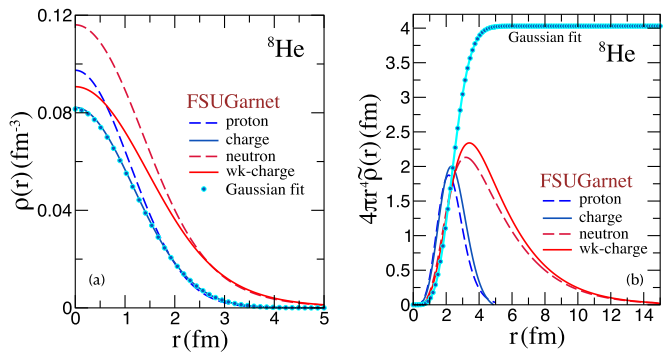

FIG. 4. (a) Proton, neutron, charge, and weak-charge densities for ^{8}He as predicted by the relativistic FSUGarnet density functional. The dots represent a one-parameter Gaussian fit to the charge density. (b) Ground-state densities suitably scaled so that the area under the curve equals the mean-square radius of the distribution.

$F_{\rm ch}(q=0)=1$. The Gaussian fit to the charge density is displayed with the small circles in Fig. 4(a). Plotted in Fig. 4(b) is a quantity for which the area under the curve equals the mean-square radius. The circles in the figure denote the cumulative (or running) sum of the charge distribution and converges to $R^2_{\rm ch}\approx(2\ {\rm fm})^2$.

So what can be concluded from comparing the experimental results against a theoretical framework that is likely being pushed beyond its limits of applicability? Insofar as the energy per nucleon is concerned, the violation of translation symmetry inherent to any mean-field-like description results in a center-of-mass correction that makes a significant contribution to the total energy of the system, calling into question the relevance of the predictions. However, COM corrections to the charge radius are relatively small [47] and comparable to the statistical error obtained in the calibration of the functional. Furthermore, the experimental value quoted in Table I is only one of three experimental determinations of the charge radius of ^{8}He. Taking into account all the measurements to date [39,42,44], one obtains at the one-sigma level an estimate of the charge radius of ^{8}He that lies in the interval $1.903\lesssim R_{\rm ch}({\rm fm})\lesssim 1.975$. This, together with the 0.03 fm theoretical uncertainty, yields a prediction for the charge radius that appears to be in reasonably good agreement with experiment. Finally, an inescapable consequence of the small one-neutron separation energy is the emergence of low-energy dipole strength in the uncorrelated (single-particle) response. How the dipole strength rearranges as a result of the inclusion of RPA correlations is the main topic of the next section.

B. Dipole response

In the previous section several ground-state properties of ^{8}He were discussed. As alluded to earlier, a self-consistent solution to the Kohn-Sham equations yields (a) single-particle energies and Dirac orbitals, (b) ground-state densities, and (c) the self-consistently determined mean-field (or Kohn-Sham) potential. Critical to the consistency of the formalism is that the potential so determined must be used without modification to generate the single-nucleon propagator from which the uncorrelated polarization tensor is obtained [31,48]. Moreover, to avoid any reliance on artificial cutoffs and truncations, the nucleon propagator (depicted by the thin line in Fig. 1) is computed nonspectrally by using Green's function methods [30].

The uncorrelated dipole response $R(\omega)$, weighted by the excitation energy ω, is displayed in Fig. 5. Clearly visible in the figure are the two sharp proton transitions involving the excitation of the $s_{1/2}$ orbital into the bound $p_{3/2}$-$p_{1/2}$ spin-orbit partners, in perfect agreement with the single-particle spectrum displayed in Fig. 2. Also shown in the figure is the emergence of low-energy dipole strength resulting from the excitation of the $p_{3/2}$ neutron orbital into the continuum. Note that among the advantages of displaying the energy-weighted dipole response is that the area under the curve is directly related to "classical" energy-weighted sum rule (EWSR) given in Eq. (4a) [32]. That is,

$$m_1\approx 14.8\Big(\frac{NZ}{A}\Big)\ {\rm MeV\ fm^2}\xrightarrow{^8{\rm He}}22.2\ {\rm MeV\ fm^2}. \qquad (6)$$

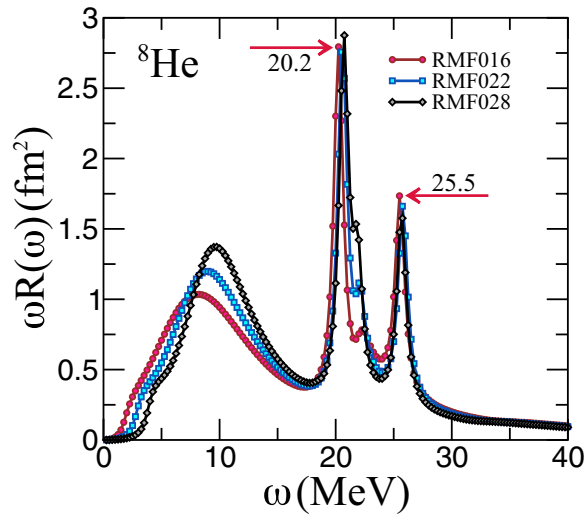

FIG. 5. Uncorrelated energy-weighted dipole response for ^{8}He for the three models considered in the text. The uncorrelated response is made up of individual particle-hole excitations with the correct quantum numbers. The arrows indicate the location of the proton excitations based on the single-particle spectrum displayed in Fig. 2.

For the uncorrelated response displayed in Fig. 5, the energy-weighted sum is predicted to be equal to 22.4, 22.6, and 22.8 MeV fm^2 for RMF016, RMF022, and RMF028, respectively in excellent agreement with the classical EWSR.

One now proceeds to discuss the RPA response, which represents the consistent linear response of the ground state to an external perturbation [30]. As depicted in Fig. 1, the RPA response goes beyond the single-particle response by building collectivity through the coherent contribution of many particle-hole pairs. Although large center-of-mass corrections preclude meaningful prediction of the ground-state energy of ^{8}He, the self-consistent RPA response offers a unique and powerful solution to the center-of-mass problem: spurious states associated with a uniform translation of the center of mass decouple from the physical modes by having their strength shifted to zero excitation energy [26]. This is particularly relevant to the distribution of isoscalar dipole ($J^\pi=1^-$, $T=0$) strength that shares the same quantum numbers as the center of mass. But given that, for nuclei with a significant neutron excess such as ^{8}He, a significant mixing between the isoscalar and isovector modes is expected, the possible emergence of a soft dipole mode will undoubtedly be affected by the decoupling of the spurious center-of-mass mode.

To investigate the mixing between modes, the distribution of isovector dipole strength obtained from a self-consistent covariant RPA calculation is displayed (on a logarithmic scale) on Fig. 6(a). Also shown is the distribution of isoscalar dipole strength predicted by the RMF028 model. As argued by Thouless [26], the spurious state associated with the translation of the center of mass is shifted to zero excitation energy. Indeed it appears that most (if not all!) of the uncorrelated isoscalar dipole strength shown in Fig. 5 is shifted to zero energy; note that the uncorrelated response is identical in both the isoscalar and isovector channels. Given the anticipated strong mixing between the isoscalar and isovector dipole modes,

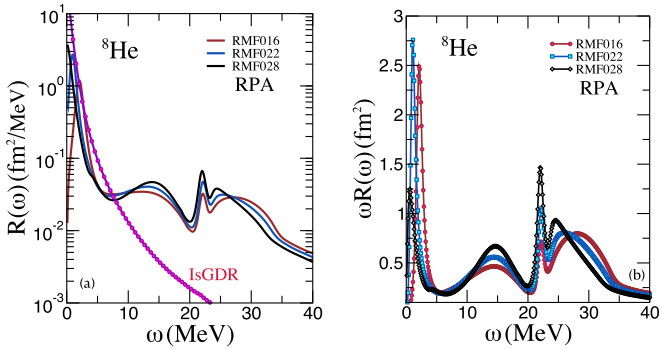

FIG. 6. (a) Correlated (RPA) dipole response for ^{8}He for the three models considered in the text. Also shown is the isoscalar dipole response to illustrate the migration of the spurious mode to zero excitation energy. (b) The narrow structures appearing at low energies in the energy-weighted RPA response are associated with the spurious center-of-mass mode.

it is reasonable to identify the narrow structures appearing at low energies in the isovector dipole response—best seen in Fig. 6(b)—as contaminants associated with the spurious center-of-mass mode. Thus, the theoretical formalism implemented here disfavors the emergence of a soft dipole mode in ^{8}He—in agreement with the conclusions from Refs. [10,11].

In an effort to remove the spurious contribution from the isovector dipole response, a smooth extrapolation to zero frequency is implemented in Fig. 7. By doing so, one can now provide estimates for the various moments of the distribution as listed in Table II. One should underscore that the estimates listed in Table II are based on the removal of the spurious strength in favor of a smooth extrapolation to zero excitation energy. This largely *ad hoc* procedure has a particularly strong effect on the electric-dipole polarizability, which is

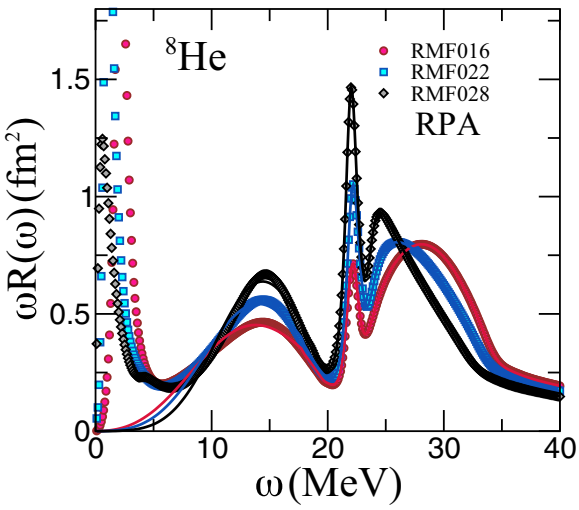

FIG. 7. Correlated (RPA) energy-weighted dipole response for ^{8}He as predicted for the three models considered in the text. The solid lines at low excitation energy represent an *ad hoc* attempt to remove the spurious strength in favor of a smooth extrapolation to zero excitation energy.

TABLE II. Estimates for various moments of the isovector dipole response of ^{8}He, as defined in Eq. (3). Also shown is the electric-dipole polarizability α_D. All these estimates are based on the smooth extrapolation to zero excitation energy depicted in Fig. 7.

Model	m_1 (fm^2 MeV)	m_0 (fm^2)	m_{-1} (fm^2/MeV)	α_D (fm^3)
RMF016	16.37	0.829	0.065	0.262
RMF022	16.70	0.849	0.060	0.242
RMF028	16.84	0.852	0.055	0.220

particularly sensitive to the low-energy part of the response because of the ω^{-1} weighting. In the case of the energy-weighted sum, the estimates are now significantly reduced relative to the classical EWSR quoted in Eq. (4a). Finally, although the information encapsulated in the various moments is valuable, there is no substitute for a direct comparison between theory and experiment of the entire dipole distribution.

IV. CONCLUSIONS

The fascinating dynamics of exotic neutron-rich nuclei has led to a paradigm shift in nuclear structure. Besides providing unique insights into the limits of nuclear existence and the production of heavy elements in the cosmos, the study of nuclei with large isospin asymmetries offers meaningful experimental constraints on the isovector sector of the nuclear interaction. In this paper the possible emergence of low-energy dipole strength in ^{8}He was investigated, a drip-line nucleus with the largest neutron-to-proton ratio known to date.

The possible existence of a soft dipole mode in ^{8}He has been a highly controversial issue, with some experiments identifying low dipole strength at an excitation energy of about 3–4 MeV [6–9] and others refuting those claims [10,11]. From the theoretical perspective, a recent *ab initio* approach that merges the Lorentz integral transform with coupled-cluster theory reports a dipole response that shows strength at about 5 MeV.

In this contribution, a theoretical formalism based on covariant density-functional theory was used to examine the emergence of low-energy dipole strength. Admittedly, using such a formalism for the study of a nucleus as light as ^{8}He is questionable. Indeed, given that center-of-mass corrections fall down slowly with mass number, they make an appreciable contribution to the total energy of ^{8}He, limiting the value of most theoretical predictions. However, the strength of DFT lies in its self-consistency. Whereas COM corrections to the ground-state energy may be large, any spurious contamination from the COM is guaranteed to decouple from the physical isoscalar dipole response [26]. This has important consequences for the isovector dipole response because the mixing between the isoscalar and isovector modes is anticipated to be strong for neutron-rich systems like ^{8}He. Hence, the narrow structures that emerged at low energies in the isovector dipole response were attributed to the shift of the spurious strength to zero—or close to zero—excitation energy. Based on this interpretation, one concludes that the emergence of a soft dipole mode in ^{8}He is disfavored by the adopted theoretical framework.

ACKNOWLEDGMENTS

The author thanks Prof. Kirby Kemper for many enlightening discussions on the many experimental efforts devoted to understand the soft dipole response of ^{8}He. This material is based upon work supported by the U.S. Department of Energy Office of Science, Office of Nuclear Physics under Award DE-FG02-92ER40750.

[1] D. Geesaman *et al.*, Nucl. Phys. News **26**, 3 (2016).
[2] D. S. Ahn *et al.*, Phys. Rev. Lett. **123**, 212501 (2019).
[3] D. Guillemaud-Mueller *et al.*, Phys. Rev. C **41**, 937 (1990).
[4] C. Hoffman *et al.*, Phys. Lett. B **672**, 17 (2009).
[5] M. Thoennessen, Rep. Prog. Phys. **67**, 1187 (2004).
[6] K. Markenroth *et al.*, Nucl. Phys. A **679**, 462 (2001).
[7] M. Meister *et al.*, Nucl. Phys. A **700**, 3 (2002).
[8] M. S. Golovkov *et al.*, Phys. Lett. B **672**, 22 (2009).
[9] L. V. Grigorenko *et al.*, Phys. Elem. Part. At. Nucl. **6**, 118 (2009).
[10] Y. Iwata *et al.*, Phys. Rev. C **62**, 064311 (2000).
[11] M. Holl *et al.*, Phys. Lett. B **822**, 136710 (2021).
[12] T. Aumann (private communication).
[13] S. Bacca, A. Schwenk, G. Hagen, and T. Papenbrock, Eur. Phys. J. A **42**, 553 (2009).
[14] M. A. Caprio, P. Maris, and J. P. Vary, Phys. Rev. C **90**, 034305 (2014).
[15] F. Bonaiti, S. Bacca, and G. Hagen, Phys. Rev. C **105**, 034313 (2022).
[16] S. Bacca, N. Barnea, G. Hagen, G. Orlandini, and T. Papenbrock, Phys. Rev. Lett. **111**, 122502 (2013)
[17] P. Hohenberg and W. Kohn, Phys. Rev. **136**, B864 (1964).
[18] W. Kohn and L. J. Sham, Phys. Rev. **140**, A1133 (1965).
[19] R. J. Furnstahl, Eur. Phys. J. A **56**, 85 (2020).
[20] T. H. R. Skyrme, Philos. Mag. (1798–1977) **1**, 1043 (1956).
[21] T. Skyrme, Nucl. Phys. **9**, 615 (1958).
[22] B. D. Serot and J. D. Walecka, Adv. Nucl. Phys. **16**, 1 (1986).
[23] J. Yang and J. Piekarewicz, Annu. Rev. Nucl. Part. Sci. **70**, 21 (2020).
[24] J. Engel, Phys. Rev. C **75**, 014306 (2007).
[25] B. Alex Brown, Phys. Rev. C **58**, 220 (1998).
[26] D. Thouless, Nucl. Phys. **22**, 78 (1961).
[27] Horst Müller and B. D. Serot, Nucl. Phys. A **606**, 508 (1996).
[28] C. J. Horowitz and J. Piekarewicz, Phys. Rev. Lett. **86**, 5647 (2001).
[29] W.-C. Chen and J. Piekarewicz, Phys. Rev. C **90**, 044305 (2014).
[30] W. H. Dickhoff and D. Van Neck, *Many-Body Theory Exposed* (World Scientific Publishing Co., Hackensack, NJ, 2005).
[31] J. Piekarewicz, Eur. Phys. J. A **50**, 25 (2014).
[32] M. N. Harakeh and A. van der Woude, *Giant Resonances-Fundamental High-Frequency Modes of Nuclear Excitation* (Clarendon, Oxford, 2001).
[33] J. Piekarewicz, Phys. Rev. C **104**, 024329 (2021).
[34] X. Roca-Maza, M. Centelles, X. Viñas, M. Brenna, G. Colò, M. Centelles, X. Vinas, B. K. Agrawal, N. Paar, D. Vretenar, and J. Piekarewicz, Phys. Rev. C **88**, 024316 (2013).
[35] P.-G. Reinhard and W. Nazarewicz, Phys. Rev. C **81**, 051303(R) (2010).
[36] J. Piekarewicz, B. K. Agrawal, G. Colò, W. Nazarewicz, N. Paar, P.-G. Reinhard, X. Roca-Maza, and D. Vretenar, Phys. Rev. C **85**, 041302(R) (2012).
[37] W.-C. Chen and J. Piekarewicz, Phys. Lett. B **748**, 284 (2015).
[38] D. Adhikari (PREX Collaboration) *et al.*, Phys. Rev. Lett. **126**, 172502 (2021).
[39] M. Brodeur *et al.*, Phys. Rev. Lett. **108**, 052504 (2012).
[40] W. J. Huang, M. Wang, F. G. Kondev, G. Audi, and S. Naimi, Chin. Phys. C **45**, 030002 (2021).
[41] M. Wang, W. J. Huang, F. G. Kondev, G. Audi, and S. Naimi, Chin. Phys. C **45**, 030003 (2021).
[42] P. Mueller *et al.*, Phys. Rev. Lett. **99**, 252501 (2007).
[43] X. Liu, P. Egelhof, O. Kiselev, and M. Mutterer, Phys. Rev. C **104**, 034315 (2021).
[44] J. J. Krauth *et al.*, Nature (London) **589**, 527 (2021).
[45] C. J. Horowitz and J. Piekarewicz, Phys. Rev. C **86**, 045503 (2012).
[46] M. Thiel, C. Sfienti, J. Piekarewicz, C. J. Horowitz, and M. Vanderhaeghen, J. Phys. G **46**, 093003 (2019).
[47] B. Mihaila and J. H. Heisenberg, Phys. Rev. C **60**, 054303 (1999).
[48] J. Piekarewicz, Phys. Rev. C **64**, 024307 (2001).